Hyperon bubble chamber (HYBUC) measurement of the Σ^+ magnetic moment

R. Settles, A. Manz, W. Matt,* T. Hansl,† I. Herynek,‡ N. Doble,§ and G. Wolf
Max-Planck-Institut für Physik und Astrophysik, Föhringer Ring 6, D-8000 München 40, Germany

S. Reucroft,¶ J. Marraffino, J. Waters, M. Webster, and C. E. Roos
Department of Physics and Astronomy, Vanderbilt University, Nashville, Tennessee 37235
(Received 4 June 1979)

We report on the final result of a precision measurement of the Σ^+ magnetic moment using the hyperon bubble chamber (HYBUC). HYBUC is a hydrogen bubble chamber with an 11.5-T superconducting magnet and was built by the Max-Planck-Institut für Physik und Astrophysik and Vanderbilt University for this experiment. A detailed description of the experiment, apparatus, and analysis is given. The final result is $\mu_{\Sigma^+} = (2.30 \pm 0.14)\mu_N$.

I. INTRODUCTION

In this paper we report on the precision measurement of the Σ^+ magnetic moment μ_{Σ^+}, performed using the hyperon bubble chamber HYBUC. The goal of the experiment was to measure μ_{Σ^+} to an accuracy of ± 0.15 nuclear magnetons (μ_N). An error of this size enables one to see the effect of baryon mass splitting on the magnetic moment.

The measurement of the magnetic moment of an elementary particle gives a measure of its internal structure without disturbing this structure. Hence, theories of elementary-particle structure can be cleanly tested by such measurements since the magnetic moments predicted by a theory vary sensitively with the assumed structure. In particular popular ideas in unitary-symmetry theories[1] or in the quark model[2] are tested by the baryon-magnetic-moment measurements. The simplest additive quark model predicts these magnetic moments correctly to within 20%, which is a considerable feat in view of the large anomalous moments these particles have. This model breaks down at the level at which the baryon magnetic moments are currently known, and other features, such as differing u, d, and s quark masses, have to be introduced.[3,4] It is important to know whether such an extended (although still simple) model can withstand the test of more accurate measurements.

In Sec. II the experimental method is reviewed; in Sec. III we describe the experimental apparatus, and in Sec. IV the data taking and analysis. In Secs. V and VI we explain the measurement of the Σ^+ magnetic moment and discuss the systematic errors. The final value of μ_{Σ^+} along with a short discussion is presented in Sec. VII.

II. METHOD

Polarized Σ^+ hyperons are produced in the reaction $K^-p \to \Sigma^+\pi^-$, the direction of polarization being known from parity conservation. The polarization precesses in the magnetic field until the Σ^+ decays. The final direction of polarization is measured using the $\Sigma^+ \to p\pi^0$ decay angular distribution, which is asymmetric due to parity violation. The precession angle is a measure of the Σ^+ magnetic moment μ_{Σ^+}.

The direction of the Σ^+ polarization at production is

$$\vec{K} \times \vec{\pi} / |\vec{K} \times \vec{\pi}| , \tag{1}$$

where $\vec{K}$ and $\vec{\pi}$ are the three-momenta of the K^- and π^-. In the Σ^+ rest frame which turns with the Σ^+ in the magnetic field, the polarization $\vec{P}$ precesses according to[5]

$$\frac{d\vec{P}}{d\tau} = \mu_a \frac{e}{mc} (\vec{P} \times \vec{B}') . \tag{2}$$

Here τ is the proper time, m the Σ^+ mass, and μ_a the anomalous magnetic moment of the Σ^+ hyperon (the units are given below); B' is the magnetic induction in the Σ^+ rest frame. The decay angular distribution is

$$\frac{1}{N}\frac{dN}{d\Omega} = \frac{1}{4\pi}(1 + \alpha \vec{P} \cdot \hat{p}) , \tag{3}$$

where N is the number of events, Ω is the solid angle, and $\hat{p}$ is the proton direction in the Σ^+ rest frame; α is the $\Sigma^+ \to p\pi^0$ decay asymmetry parameter and $\vec{P}$ is the polarization at the point of decay. The circumflex denotes a unit vector. We use the coordinate system $\hat{z} = \hat{B}'$, $\hat{y} = \hat{B}' \times (\hat{P}_0 \times \hat{B}')/|\hat{P}_0 \times \hat{B}'|$, and $\hat{x} = \hat{y} \times \hat{z}$, where $\hat{P}_0$ is the direction of the polarization at the decay vertex for $\mu_a = 0$. Thus $\hat{z}$ is the normal to the plane of precession, $\hat{y}$ is the projection of $\hat{P}_0$ onto the precession plane, and $\hat{x}$ is the third axis. For HYBUC $\hat{P}_0$ lies approximately in the precession plane as shown in Fig. 1, which demonstrates the coordinates and angles used. If the decay-proton direction is specified by the spherical coordinates θ and ϕ, θ being the polar angle with respect to the $\hat{z}$ axis and ϕ the

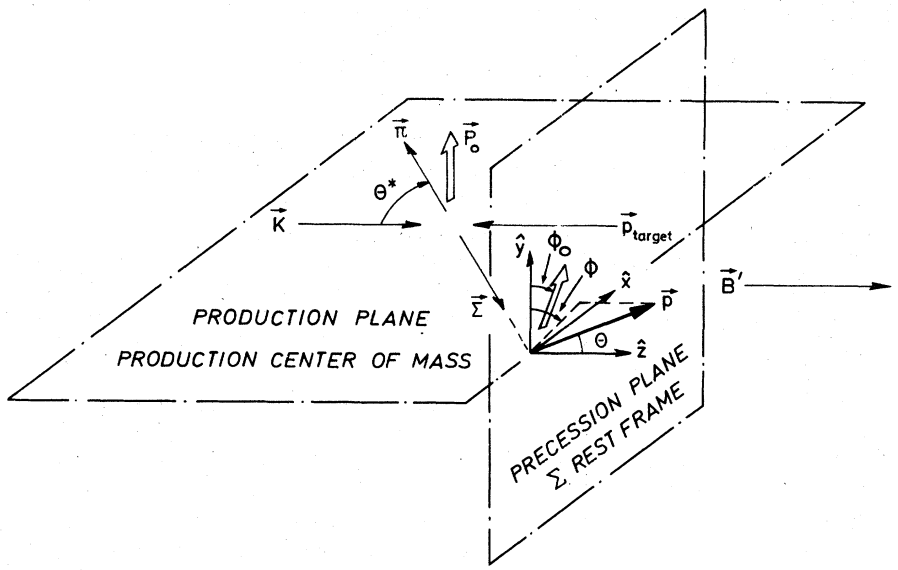

FIG. 1. Coordinate system used for the μ_{Σ^+} measurement and definition of $K^-p \to \Sigma^+\pi^-$ production and $\Sigma^+ \to p\pi^0$ decay angles.

azimuthal angle in the precession plane measured from the $\hat{y}$ axis, the distribution Eq. (3) becomes

$$\frac{1}{N}\frac{dN}{d\Omega}=\frac{1}{4\pi}[1+\alpha P_\perp \sin\theta\cos(\phi-\phi_0)+\alpha P_z\cos\theta], \tag{4}$$

with $P_\perp=(P_x^2+P_y^2)^{1/2}$. For a Σ^+ sample with proper lifetime $c\tau$, the magnetic moment μ_a is calculated from the precession angle

$$\phi_0=\mu_a\frac{e}{mc^2}c\tau B', \tag{5}$$

where the units are such that μ_a is in intrinsic magnetons, i.m., $e/mc^2=0.002\,521\ \text{cm}^{-1}\ T^{-1}$, $c\tau$ is in cm, and $B'=|\vec{B}'|$ is in T. The total magnetic moment is

$$\mu_{\Sigma^+}=(\mu_a+1)(m_p/m)\ \mu_N,$$

where m_p is the proton mass. The error on the anomalous magnetic moment is given approximately by[6]

$$\delta\mu_a\approx(0.002521\, c\tau_0\,\alpha P\sin\beta B'\sqrt{N})^{-1}, \tag{6}$$

where β is the angle between $\vec{P}$ and $\vec{B}'$ and $c\tau_0=2.4$ cm is the mean Σ^+ lifetime.

III. EXPERIMENTAL APPARATUS

The hyperon bubble chamber HYBUC was built by the Max-Planck-Institut für Physik und Astrophysik and by Vanderbilt University for this experiment. HYBUC is a liquid hydrogen bubble chamber with a useful volume 32 cm long and 11 cm in diameter, surrounded by an 11-T superconducting solenoid. Figure 2 shows an overall sketch of the detector.

Seven previous experiments[7] to measure μ_{Σ^+} had measuring accuracies around $\pm1\ \mu_N$. Various experimental techniques had been used including emulsion and spark chambers with pulsed magnetic fields of some tens of T and bubble chambers with dc fields of up to 4.5 T. Our choice of a hydrogen bubble chamber with a high-field superconducting magnet was made after several months of study. We now review briefly the reasons for choosing this apparatus to measure μ_{Σ^+} and then give a description of the setup.

A. Choice of technique

The physical principles for all μ_{Σ^+} experiments to date were described in Sec. II. These principles led to the following requirements on our apparatus:

(i) The detection efficiency should be as nearly isotropic as possible in order to keep any bias on observing the hyperon production and decay to a minimum.

(ii) The measuring accuracies of angle, momentum, and Σ^+ track length should be high enough so that the error on measuring ϕ is as small and as free from bias as possible.

(iii) For maximum precession and accuracy, the polarization and magnetic field should be perpendicular to one another [see Eqs. (2) and (6)].

(iv) The magnetic field should be as large as possible to make $\delta\mu_{\Sigma^+}$ as small as possible [Eq. (6)].

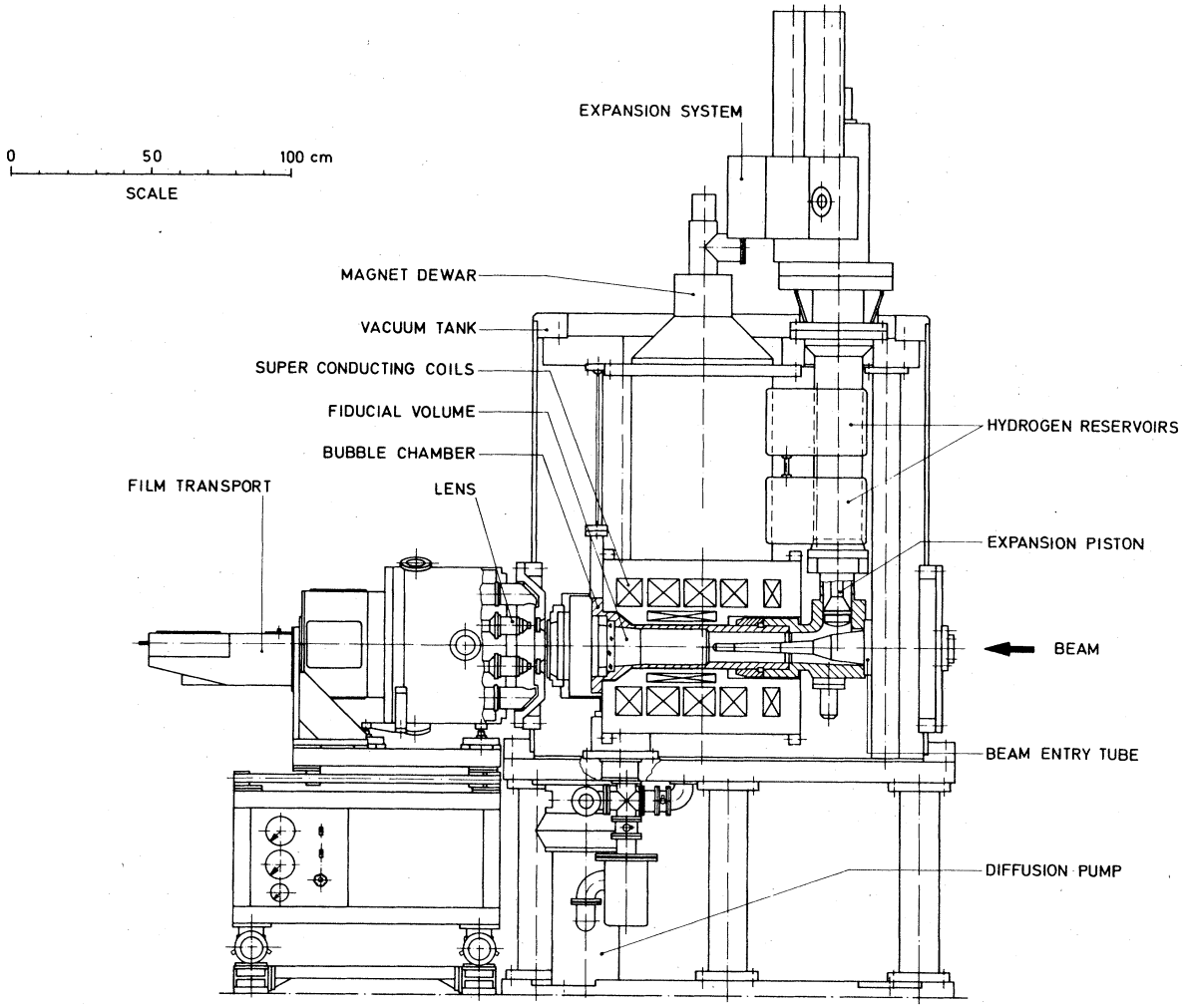

FIG. 2. Overall sketch of the HYBUC apparatus.

(v) Similarly, the product $|\alpha P\sqrt{N}|$ for the hyperon production and decay should be as large as possible [Eq. (6)].

The requirements (i) and (ii) led to the choice of a hydrogen bubble chamber as particle detector. The early emulsion experiments were designed to observe not the Σ^+ production point but only its decay, so that the overall length of an individual Σ^+ could only be estimated, and, moreover, the topology of the $\Sigma^+ \to p\pi^0$ decay was very similar to the more frequently occurring proton elastic scatter. The spark chamber experiments had an anisotropic efficiency for detecting the hyperon decay. In a liquid hydrogen bubble chamber, both the production and decay vertices are seen with nearly uniform efficiency in space. The clean kinematic fitting in hydrogen and the ionization information fix the identity of the particles. Moreover, the measuring accuracy is excellent; in HYBUC ϕ is measured to $\pm 1°$ on average.

Requirement (iii) meant that the K^- beam must enter the apparatus along the magnetic field direction. This beam direction is unconventional for bubble chambers, but it results in the angle β in Eq. (6) being 90° for all directions of Σ^+ production. It also eliminates any problems of getting the beam into the high-field region. This choice of beam direction had little effect on standard scanning, measuring, and reconstruction procedures. A typical event may be seen in Fig. 3.

Requirement (iv) led to the design of an 11-T, 6-in. bore superconducting solenoid for the experiment. A solenoidal rather than a Helmholtz configuration gives maximum possible field strength at the center of the magnet and is well matched to the axial beam entry. A superconducting magnet was chosen as opposed to a pulsed magnet, which could have reached higher field strengths,

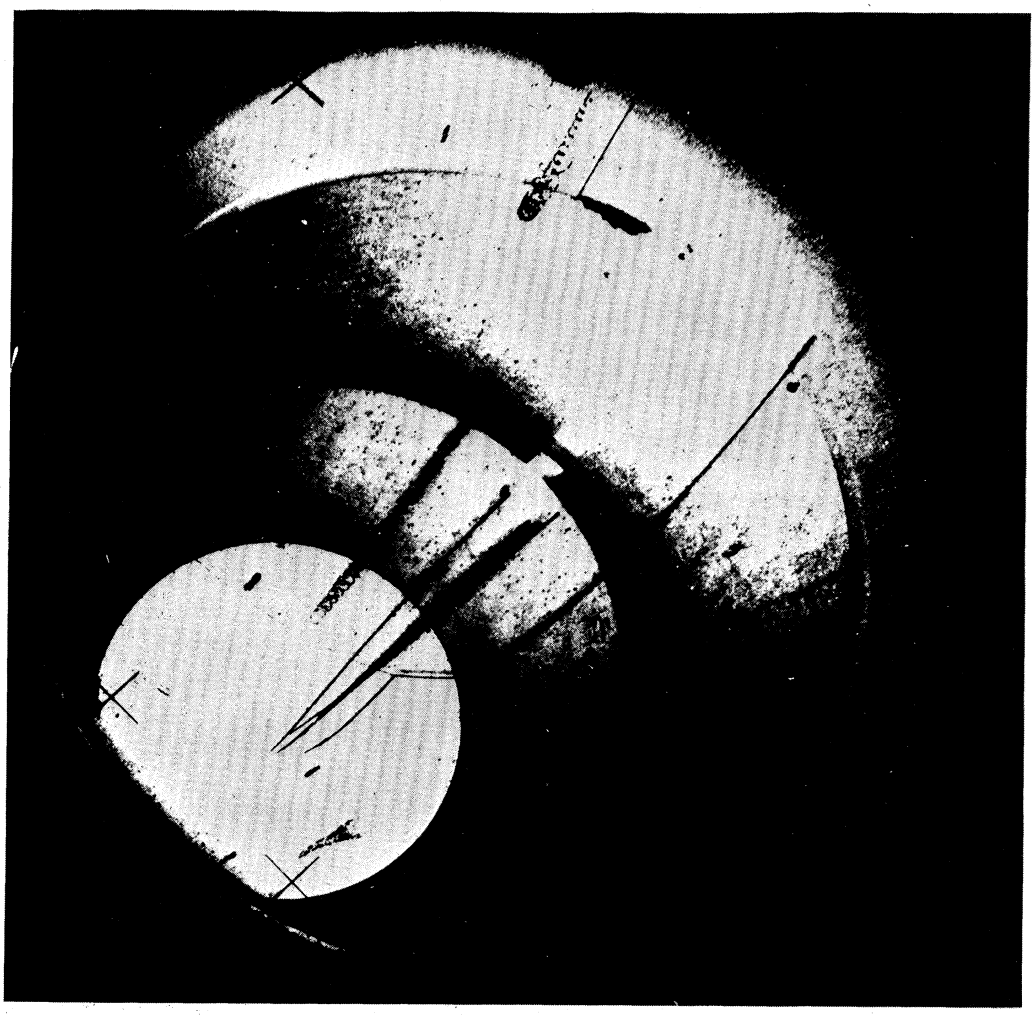

FIG. 3. A typical $K^-p \to \Sigma^+\pi^-$, $\Sigma^+ \to p\pi^0$ event in HYBUC.

because of the technical difficulties in constructing and operating a bubble chamber with a pulsed magnet.[8] The maximum field strength at the superconductor is limited by the current vs field characteristic of the superconductor (the so-called "short-sample limit"). The field strength at the magnet center is then a function of the diameter of the solenoid. The size needed for the magnet and bubble chamber is determined by the track length necessary to have enough measuring accuracy as required by (ii) above. The central field strength and size of HYBUC were chosen such that the tracks had roughly optimum lengths, viz., the length at which multiple scattering starts to dominate the measuring accuracy in momentum and angles. The final solution of 11 T over a 6-in bore was (and still is) at the technological limit.

Requirement (v) demanded finding the Σ^+ production reaction and decay channel for which the product $|\alpha P\sqrt{N}|$ is a maximum. A study using results from phase-shift analyses[9] led us to choose the already mentioned reaction.

$$K^-p \to \Sigma^+\pi^- \quad (7)$$
$$\searrow p\pi^0$$

at beam momenta of 420–500 MeV/c. For some 10^7 K^- (corresponding to about 2×10^6 pictures) at this momentum incident on 20 cm of liquid hydrogen in an average field of 10 T, Eq. (6) gives an expected error of $\pm0.15\mu_N$, an improvement by a factor of 7 over any previous measurement.

A final point relating to (i), the detection efficiency, should be made here. Events having too small an angle between the Σ^+ and the decay product in the laboratory frame will be lost in scanning the film. We therefore expected (and found) a loss of $\Sigma^+ \to p\pi^0$ events with a lab decay angle less

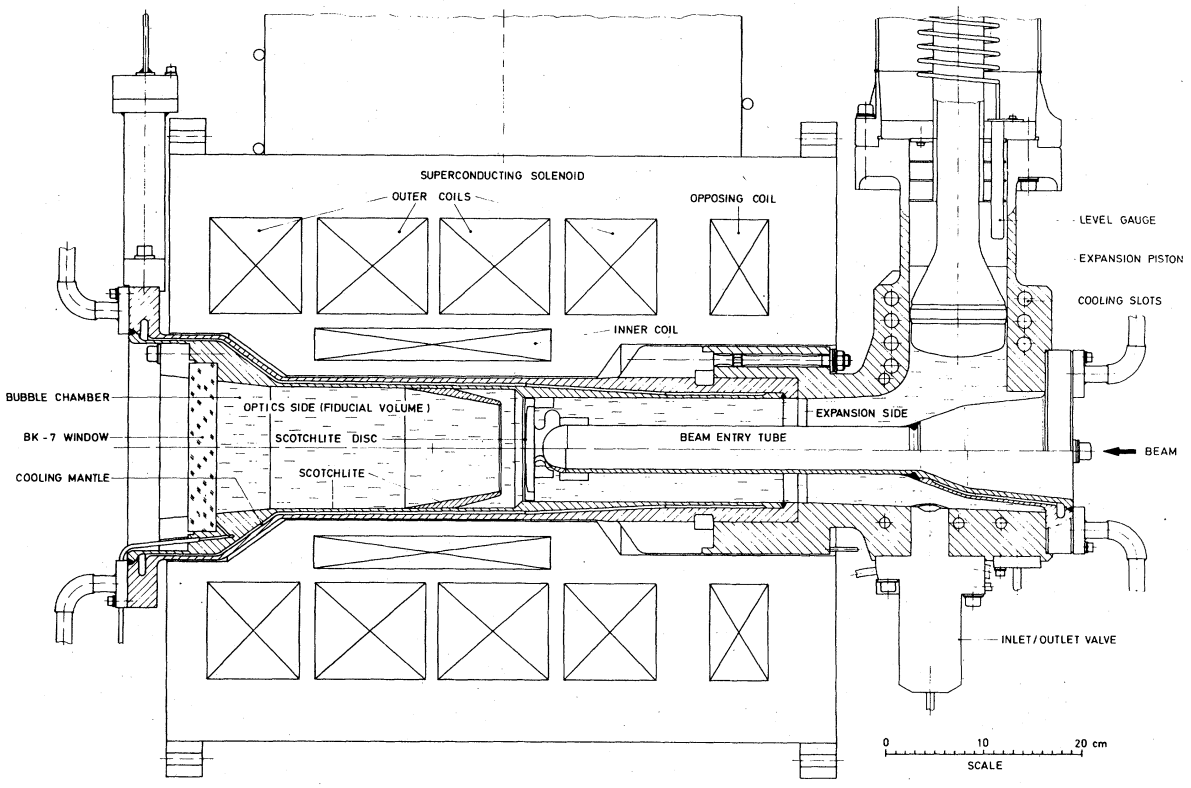

FIG. 4. Close-up sketch of the bubble chamber and superconducting solenoid.

than about 5°. This loss biases the μ_D+ measurement, but the bias for events with positive magnetic-field direction is opposite to that for events with negative magnetic-field direction. (Positive field points downstream along the beam, negative field upstream.) The bias cancels in a sample having the same numbers of positive- and negative-field events. The design of the experiment thus included the plan to take half of the data with positive and half with negative field.

B. Description of the apparatus

Figure 4 shows a sketch of the bubble chamber and magnet assembly. The superconducting solenoid was a composite magnet with 15 NbTi outer coils and a Nb_3Sn inner coil. Its overall length was 59.1 cm and the inside (outside) diameter was 18.5 cm (48.6 cm), winding to winding. The NbTi coil at the beam entry end of the chamber was an opposing coil, wound in the opposite sense to the others in order to provide a low field region for the beam entry. Technical features of the magnet system include mechanical design which emphasized strength at the expense of having poor helium ventilation, copper oxide coating for insulation, twisted filaments in the NbTi composite portion, and interleaved high purity Al foils in high radial field regions of the Nb_3Sn tape wound portion to dampen flux penetration. The ouside of the magnet dewar was refrigerated with liquid hydrogen, and the overall liquid helium consumption (transfer plus boil-off losses) was about 10 l/h. The magnet system reached 11.7 T in tests; for data taking the field values used were 11.1 and 11.4 T. The magnet operated about 5000 h at the latter field levels. These field levels were within a few percent of the short-sample limit (11.8 T), so that the charging of the magnet had to be done very carefully and took half a day. A complete description of the magnet design and operation has been published.[10]

The bubble-chamber body divided roughly into two parts as can be seen in Fig. 4: the optics side consisting of the fiducial volume in the high field region and the expansion side. The chamber body actually was made of two parts which were fed in from either side of the solenoid and bolted together. The fiducial volume contained 4 l and the entire volume 14 l of liquid hydrogen. The solenoid magnet design permitted no other choice than to place the expansion piston outside the magnet, and the solution as seen in Fig. 4 resulted. The optics side was closed with a 3-cm-thick window made

of BK-7. The expansion side was fitted with a beam entry tube which permitted the K^- beam to enter the chamber up to the fiducial region before encountering liquid hydrogen. The chamber volume was surrounded by a cooling mantle for temperature control; the cooling mantle was implemented on the optics side by a two-concentric-cylinder design and on the expansion side by cooling slots. Static pressure was controlled via an inlet above the piston. The walls of the fiducial volume were covered with Scotchlite[11] for illuminating the tracks. There were 12 fiducial marks placed on the BK-7 window and five on the chamber body for use in the geometrical reconstruction of the events. The optics and expansion volumes were separated by a Scotchlite covered disk which moved with each expansion. Typical chamber operating conditions were 26° K, 1 bar overpressure, expanded pressure about 1.2 bar, and flash delay 1 msec.

It was decided to photograph the chamber with five views in order to avoid hidden regions of the chamber and to have redundancy for handling the unconventional beam direction. This beam direction led to a larger proportion of highly dipping tracks than normally encountered in bubble-chamber experiments; hence, in order to measure as accurately as possible in depth, the stereo angle was made as large as possible. In the final solution, seen in Fig. 2, the aperture stop of each of the five views is 30 cm from the BK-7 window. Laterally to the chamber axis, four of the views were positioned on the corners of a square and 10 cm from the chamber axis, and the fifth view was on the chamber axis. The stereo angle for diagonally opposing views varied from 18° to 34° over the depth of the chamber. The optical axes of all five views were parallel to one another. Such an arrangement meant that the field of view extended up to 30° (half angle). This was possible by allowing a certain amount of distortion, which was 10% at the extremity of the field of view. The optical system for each view was essentially an inverted telescope consisting of two lenses with intermediate imaging. The first lens formed the intermediate image, and the second lens transported the image to the film plane about 1 m from the high-field region. The first lens was designed for an aperture stop 23 mm in front of the first lens surface. The diameter of the aperture stop was 1.1 mm to give the necessary depth of focus. The size of the Airy disk at half height was 250μ, and this is the size to which the bubbles were grown. The image transporting enabled the introduction of a system of parallel mirrors for shifting the images from all five views to be adjacent to one another on the same strip of film. In this way only a single film transport was necessary. Each of the four outer views had a separate flash which was imaged onto a small mirror 5 mm from the aperture stop where it was the light source for the bright-field illumination. The on-axis view had no flash of its own. The four flashes of the outer views delivered enough light to give a bright image of the bubbles in the on-axis view, while at the same time the amount of light scattered directly from the Scotchlite into this view was less than that from the bubbles. The on-axis view thus had a dark-field illumination: bright bubbles on a gray background.

The expansion was completely forced, driven by an hydraulic actuator. This actuator was steered by a precision servovalve which followed the command of an electrical stroke-time input function. A 9-msec expansion cycle was normally used. The expansion piston was a fiberglass reinforced epoxy design 10.4 cm in diameter. An expansion by 0.7% volume necessary for track sensitivity corresponded to a 12 mm stroke. The piston rod assembly had a mass of 11 kg, giving rise to a three-ton dynamic force with each expansion.

The bubble chamber, expansion system, and magnet were suspended from the upper plate of the vacuum safety tank surrounding the cold part of the apparatus. The overall refrigeration of the bubble chamber and outer magnet dewar wall was delivered by a 320-W hydrogen refrigerator.

The 420–500 MeV/c K^- beam is shown in Fig. 5. It was derived from an internal target in the CERN proton synchrotron (PS) ring. It was a two-stage electrostatically separated beam 16 m long. The first 1-m electrostatic separator removed the π^- from the beam, the second removed the μ^-. Pairs of quadrupoles at the beginning and end of the beam focused the beam; a single quadrupole at the middle acted as the field lens. There were two focal points, one at the field lens and one at HYBUC. Two bending magnets provided momentum analysis. The two successive deflections with intermediate focus gave momentum recombination. The final focused image was pencil-sized, 4 mm in diameter. Achieving such a pencil beam required designing for the corrections for dispersion and chromatic aberration, strict conditions being imposed on the optics, lengths, and bending angles in the beam. It also meant careful work in tuning the beam. The pencil focus allowed for very effective background shielding at the bubble chamber. The focus was placed 50 cm upstream of the fiducial volume in the beam entry tube so that the K^- particles entered the fiducial volume well separated from each other within about a 2-cm-diameter circle. The momentum bite was ±1% and the emittance was $\pm(2 \times 20)$ mm mrad. The μ contamination in the beam was very low—less than 10%.

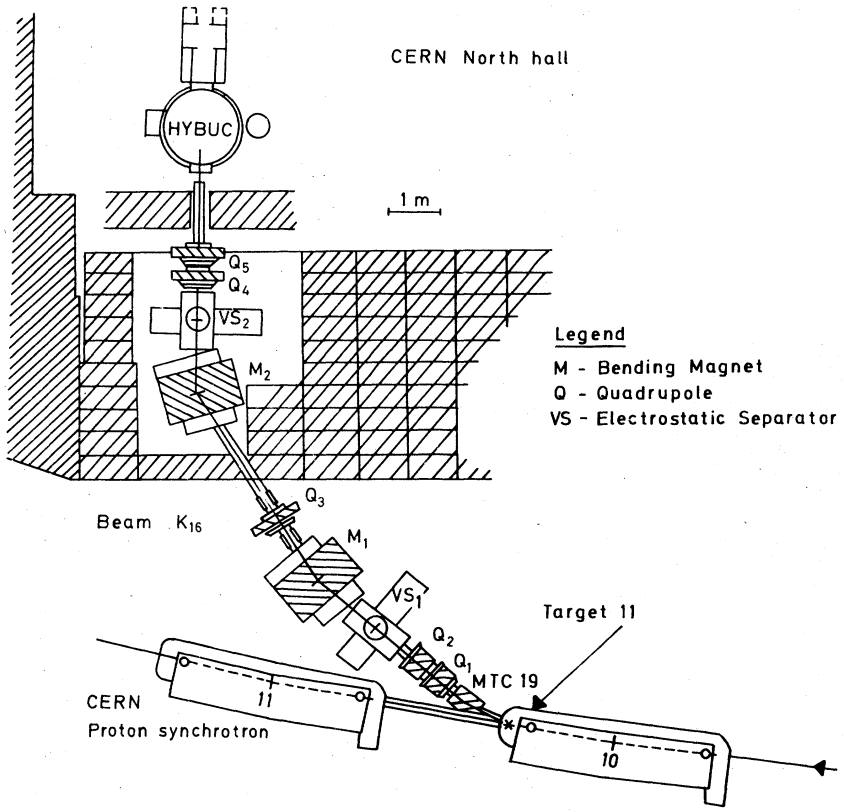

FIG. 5. Layout of the K^- beam in the North Hall of the CERN proton synchrotron.

The PS circulating beam was steered onto the internal target for 300 μsec in such a way that about 10^{11} protons at 20 GeV interacted in the target. This gave an average flux of about 8 K^- per picture.

IV. DATA TAKING AND ANALYSIS

A total of 2.4 million pictures were taken at the CERN PS in 2500 h of running. Approximately 20% of the pictures were discarded because of poor beam and/or chamber conditions, almost all of the discarded films coming from the very early days of the running. An average of about 8 K^- per picture were used, so that the total exposure encompassed 1.5×10^7 K^- in the analyzed pictures.

Data were taken at nominal beam momenta of 440, 460, 480, and 500 MeV/c, the ratio of pictures taken at the different beam momenta being approximately 1:6:4:3. The field direction was switched from positive (along the beam) to negative, and vice versa, from time to time in order to have about the same number of events with positive field as with negative field. This was very important since all significant systematic biases in measuring μ_{Σ^+} are opposite for the two field directions and therefore cancel in a final sample having equal statistics for the two field directions.

The good films were scanned twice for the two-prong-$V^\pm$ topology, and the events were measured on manual machines both at the Max-Planck-Institut für Physik und Astrophysik and at Vanderbilt University. The measurements were processed by the HYDRA[12] geometry-kinematics reconstruction program. Each event, together with the program results, was then reexamined on the scanning tables. The ionization of the tracks was used to decide between the hypothesis

$$K^-p\to\Sigma^+\pi^- \;(\Sigma^+\to p\pi^0)\quad,\quad K^-p\to\Sigma^+\pi^- \;(\Sigma^+\to n\pi^+)\quad,\text{ and }\quad K^-p\to pK^- \;(K^-\to pp\to pp)$$

for the positive V's. All events which failed to give an acceptable multivertex kinematic fit in agreement with the ionization decision were remeasured, and those events which still failed were remeasured again. The residual failure rate for these Σ candidates was less than 5% after this procedure. A subsequent study showed that at most 10% of these failing events (i.e., $<0.5\%$ of the total sample) were two-body Σ events. The overall scanning efficiency calculated statistically was better than 99%. There was also a 7% systematic loss of $\Sigma^+\to p\pi^0$ events with small decay angle or with a

decay track too short to detect; this loss will be treated in detail in the next section.

A considerable amount of work went into the analysis program chain. The magnetic field was mapped four different times during the running to check constancy and reproducibility of the magnet. These field maps showed that the magnet did not change during the experiment and were the data for calculating the magnetic-field constants for the geometry-reconstruction program. About half the data were taken with the opposing coil and half without, and in each of these data samples about half of the film was taken with positive- and half with negative-field direction. Thus there were four magnetic fields to compute.

Similarly the optical distortion for each objective had to be mapped. These optical maps plus measurements of fiducial marks and event vertices on film taken during the running were used to generate optical constants for the geometry program. The film was exposed in ten separate two-to-three-week runs. Before each run the bubble chamber was cleaned, which meant dismounting and remounting the BK-7 window, after which new optical constants were necessary. For each of the runs a set of theodolite measurements were made to determine the position of the bubble-chamber fiducial volume relative to the magnetic field and to use in computing optical constants. Thus there were ten sets of optical constants to be made. In addition the four different beam momenta used required four sets of beam constants to be determined. This resulted in a total of 18 different sets of magnetic field, optics, and beam constants to be tuned along with the programs.

A large effort was invested in the development and optimization of the HYDRA geometry and kinematics programs since this was one of the first experiments to use them. This brief mention hardly does justice to the debugging work done, but eventually the programs, together with the final magnetic field and optical constants, ran very reliably. The point-reconstruction error was 70 μm in space.

V. MEASUREMENT OF THE Σ MAGNETIC MOMENT

The fiducial volume extends from 2 cm downstream of the Scotchlite disk at the entrance to 6 cm upstream of the BK-7 window at the exit of the chamber. Events inside this fiducial volume are within the high-field region and have decay tracks which are long enough to be well measured.

Only events with a Σ^+ track longer than 3 mm are used for determining μ_{Σ^+}. Events with a short Σ^+ track were more difficult to find and measure than events with a long Σ^+ track. Also Σ^+'s with a track shorter than 3 mm would contribute practically nothing to the accuracy of measuring μ_{Σ^+} since the precession angle for a Σ^+ is roughly proportional to its length.

The events used are required to have a missing mass recoiling from the π^- at the $K^-p \to \Sigma^+\pi^-$ production vertex between 1.15 and 1.23 GeV/c^2. This eliminates events with an off-momentum beam track and those with an additional π^0 at production, $K^-p \to \Sigma^+\pi^-\pi^0$.

Integrating Eq. (4) over θ,

$$\frac{1}{N}\frac{dN}{d\phi} = \frac{1}{2\pi}\left[1 + \frac{\pi}{4}\alpha P_\perp \cos(\phi - \phi_0)\right] \tag{8}$$

is the expected distribution for ϕ. After the selection described above, 24 513 events of the type in

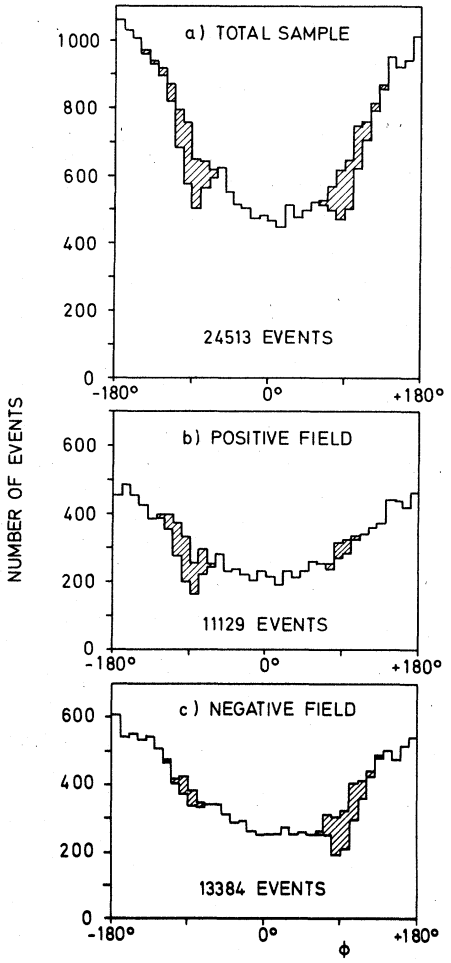

FIG. 6. Distribution of the decay angle ϕ, Eq. (8), for the total sample of $\Sigma^+ \to p\pi^0$ events: (a) all events, (b) events with positive field direction, and (c) events with negative field direction. Open histogram: raw data. Cross-hatched area: after weighting the region of losses by Monte Carlo (see discussion in text).

Eq. (7) remain, and their ϕ distribution is shown in Fig. 6(a), open histogram. The holes at +90° [predominantly in negative-field events, Fig. 6(c), open histogram] and −90° [predominantly in positive-field events, Fig. 6(b), open histogram] are due to the 7% decay losses mentioned in the preceding section and to be discussed now.

There are in fact three sources for these losses. Firstly, there are events for which the angle between the Σ^+ and the decay proton as projected onto the film plane is too small to be seen and which therefore look like elastic scatters $K^-p \to K^-p$. Secondly, there are a few events for which the decay proton is too slow to leave a visible track. These events also look like elastic scatters. Thirdly, only events for which both vertices could be well measured in at least two views are accepted. This third source of loss is unavoidable since the positions of the vertices are so important for the μ_{Σ^+} measurement. The positions of the production and decay vertices of a Σ^+ are needed to determine its lifetime and track parameters, in particular the Σ^+ turning angle. Both the lifetime and the turning angle are used directly in the magnetic-moment calculation.

We have three methods for dealing with these losses:

(a) Do nothing and depend on the fact that the losses bias μ_{Σ^+} in the opposite sense for opposite field directions, so that when all data are taken together the systematic effects cancel and the final result is unbiased.

(b) Cut out completely the region of losses in the ϕ distribution and correct the likelihood function for the cut.

(c) Use a Monte Carlo calculation to weight the experimental distribution in the variables showing the losses most clearly and thereby fill in the holes.

Method (a) makes use of the symmetries built into the experiment for avoiding bias (see Secs. III A and IV). Of course this bias canceling also holds for methods (b) and (c): Any systematic effects left after cutting, (b), or weighting, (c), will tend to cancel when all data are combined. Method (b) has the advantage that is completely independent of μ_{Σ^+} but has the disadvantage that the cutting reduces the number of events and increases the error slightly. Method (c) uses the full statistics and makes the distributions smooth after weighting but has the drawback that the weights depend on the value of μ_{Σ^+} used in generating the Monte Carlo events. This dependence, however, turns out to be slight since we only weight the region of losses and leave the rest of the distribution untouched. The μ_{Σ^+} results for all three methods will be seen to be the same well within errors.

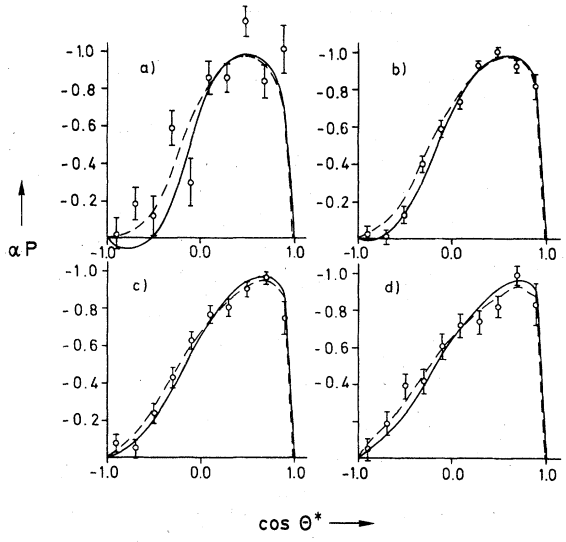

FIG. 7. Variation of αP with $\cos\theta^*$ for the $K^-p \to \Sigma^+\pi^-$, $\Sigma^+ \to p\pi^0$ events at the four nominal beam momenta (a) 440 MeV/c, (b) 460 MeV/c, (c) 480 MeV/c, and (d) 500 MeV/c. The curves show the predictions of the partial-wave analyses of Ref. 14: solid line, Hepp *et al.*, and dotted line, Gopal *et al.*

From Eqs. (8) and (5) we can write down the contribution to the likelihood function for the ith event

$$L_i = 1 + \frac{\pi}{4}\alpha P_i \cos\left(\phi_i - \mu_a \frac{e}{mc^2} c\tau_i B'_i\right). \qquad (9)$$

The decay asymmetry parameter is $\alpha = -0.978$ according to the Particle Data Tables.[13] The polarization P_i for an event is calculated from the π^- production angle θ_i^* using the coefficients found in K^-p reaction partial-wave analyses,[14] the results of which fit our data very well.[15] This can be seen in Fig. 7, which compares $\alpha P(\cos\theta^*)$ of this experiment with that of the partial-wave analyses. The π^- production angle θ^* is defined in Fig. 1. The numbers ϕ_i and $c\tau_i$ in Eq. (9) are calculated from the results of the geometrical vertex fit and the multivertex kinematical fit for the event. The value for B'_i is calculated from the average magnetic field over the Σ^+ track and the average momentum of the Σ^+. The function $\sum_i \ln L_i$ is formed for all events of a sample, and the magnetic moment for this sample is that value of μ_a for which this function is a maximum. The error on the magnetic moment is given by the values of μ_a for which the function $\sum_i \ln L_i$ decreases by 0.5 from the maximum.

The magnetic-moment measurement is most sensitive to events with large polarization. We therefore further select our data as a function of the center-of-mass production angle θ^* to isolate

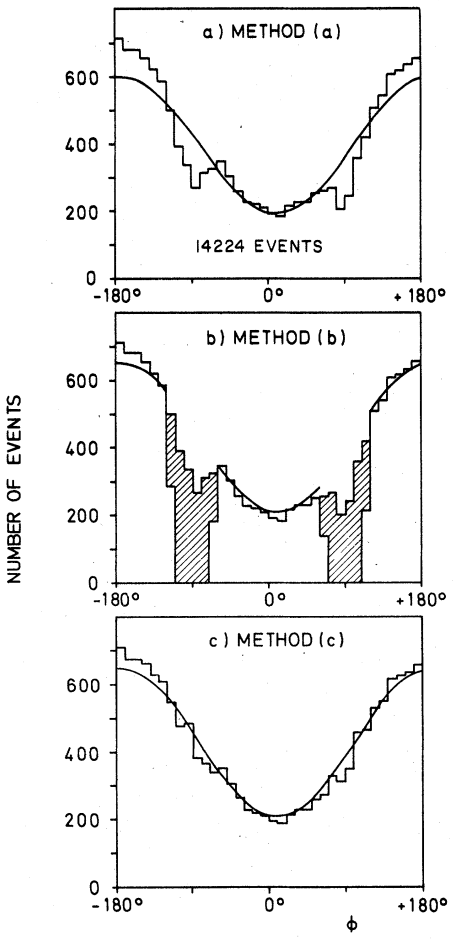

FIG. 8. Experimental (histogram) and fitted (smooth curve) distributions of the decay angle ϕ for the $\Sigma^+ \to p\pi^0$ events with $\cos\theta^*$ selection for the methods (a), (b), and (c) described in the text: (a) no correction for small angle decay losses, (b) cutting the region of loss (cross-hatched area) out of the data, and (c) weighting the region of losses by Monte Carlo.

the region of high polarization. The selected events have $-0.5 < \cos\theta^* < +0.75$ (see Fig. 7). This cut eliminates the kinematic region with very fast and very slow Σ^+. It also eliminates those events discussed earlier which have a proton track too short to be seen. This procedure reduces our statistics from 24 513 events to 14 224 events but increases the error $\delta\mu_{\Sigma^+}$ by only about $0.01\mu_N$. This cut also reduces the effect of the zero-constraint ambiguities from 2.5% of the total sample to 0.7% of the selected one. These ambiguities are due to decay particles (p or π^+) traveling along the field. Such events have three kinematic solutions (high-momentum proton, low-momentum proton, and pion) and have a ϕ angle +90° (positive field) or −90° (negative field).

Using this event sample of 14 224 events with the $\cos\theta^*$ selection, the three methods (a), (b), and (c) described above give the following results:

(a) Maximizing the likelihood function for the sample with $\cos\theta^*$ selection, making no attempt to correct for the small-angle decay losses, yields $\mu_{\Sigma^+} = (2.35 \pm 0.14)\mu_N$. Figure 8(a) shows the ϕ distribution for these events with the curve corresponding to this value of μ_{Σ^+}. The total sample of 24 513 events without $\cos\theta^*$ selection gives the value $(2.37 \pm 0.13)\mu_N$.

(b) Cutting out of the ϕ distribution the regions with losses ϕ_1 to ϕ_2 and ϕ_3 to ϕ_4 requires renormalizing the expression in Eq. (8):

$$\frac{1}{N}\frac{dN}{d\phi} = \frac{1}{K}\left[1 + \frac{\pi}{4}\alpha P_\perp \cos(\phi - \phi_0)\right],$$

where

$$K = 2\pi + \phi_1 - \phi_2 + \phi_3 - \phi_4 \qquad (10)$$
$$+ \frac{\pi}{4}\alpha P_\perp [\sin\phi_0(\cos\phi_2 - \cos\phi_1 + \cos\phi_4 - \cos\phi_3)$$
$$- \cos\phi_0(\sin\phi_2 - \sin\phi_1 + \sin\phi_4 - \sin\phi_3)].$$

For the positive- (negative-) field sample, events within ±30° of $\phi = -90°$ (+90°) and within ±20° of $\phi = +90°$ (−90°) were cut out of the distribution. These cuts are large enough that no discernible losses are left [see Figs. 6(b) and 6(c)]. The maximum-likelihood analysis using Eq. (10) to define the likelihood function then gives the value $\mu_{\Sigma^+} = (2.26 \pm 0.17)\mu_N$. Figure 8(b) shows the ϕ distribution for the events with $\cos\theta^*$ selection with the curve corresponding to this value of μ_{Σ^+}. The cross-hatched regions are those affected by the ϕ cuts.

(c) The third method is to correct for the losses by weighting experimental distributions to agree with those calculated using the Monte Carlo technique. The first task was to find which variables showed the losses most clearly since the weighting is best done in those variables. Two variables are used; the first, which we call $\phi_{\rm dif}$, is the difference between the Σ^+ and the proton laboratory angles projected onto the film plane, and the second is the Σ^+ length l_Σ. The first variable $\phi_{\rm dif}$ is approximately the angle seen by the scanner, so that it is obvious that here the losses should show up clearly. It is necessary to weight also as a function of l_Σ since the losses in $\phi_{\rm dif}$ are a bit larger for short Σ's than for long ones. The distribution in $\phi_{\rm dif}$ is seen in Fig. 9, open histogram. The hole at $\phi_{\rm dif} = 0°$ shows the small-angle decay loss. Some of the events with $\phi_{\rm dif}$ near 0° are identified in one or more of the four outer views of HYBUC, and some are identified as a result of different Σ^+ and proton track characteristics.

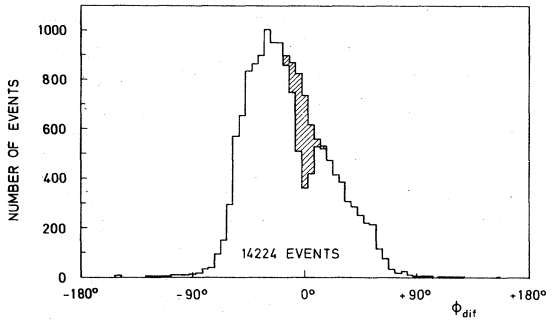

FIG. 9. Distribution for the final $\Sigma^+ \to p\pi^0$ event sample (with $\cos\theta^*$ selection) in ϕ_{dif}, the difference of the angles of the Σ^+ and the proton tracks as projected onto the film plane. Open histogram: raw data. Cross-hatched area: after weighting by Monte Carlo.

Thus the hole at $\phi_{dif} = 0°$ does not go to zero.

The inputs to the Monte Carlo calculation for a given sample were $K^- p \to \Sigma^+\pi^-$ reaction kinematics, the Σ^+ decay distribution of Eq. (8), the HYBUC geometry, the experimental beam momentum distribution and the beam energy loss in the chamber, the $K^- p \to \Sigma^+\pi^-$ reaction angular distributions and the Σ^+ polarizations, both determined from the above-mentioned partial wave coefficients,[14] the exponential decay law with $c\tau_0 = 2.4$ cm, the energy loss of the Σ^+, the HYBUC magnetic-field map, the fiducial volume and Σ^+ length cuts described at the beginning of this section, and the Σ^+ anomalous magnetic moment $\mu_a = 2$ i.m. (corresponding approximately to the result of method (a) above). The effect of this choice for μ_a on the final result as opposed to an alternative realistic value is practically negligible and is discussed in the next section.

For the weighting procedure, the data were divided into eight samples corresponding to the four field maps from two laboratories. The data were further divided into four intervals according to l_Σ such that the events from each interval gave a value of μ_{Σ^+} with about the same accuracy ($\approx \pm 1 \mu_N$). For each sample and l_Σ interval, the ϕ_{dif} distribution was plotted for the experimental and for the Monte Carlo data, the ϕ_{dif} bin width being 5° (as in Fig. 9). The experimental data were weighted in the region $-10° \lesssim \phi_{dif} \lesssim +10°$ by the ratio of the number of Monte Carlo events to the number of experimental events for each ϕ_{dif} bin. The Monte Carlo data were normalized to the experimental data outside the region being weighted. The effect of the weighting on the data is seen by the cross-hatched areas in Figs. 6(a), 6(b), and 6(c) and in Fig. 9.

The maximum-likelihood fit to the weighted experimental data yields a magnetic moment of $\mu_{\Sigma^+} = (2.29 \pm 0.14)\mu_N$. The weighting has been properly accounted for in computing the error. Figure 8(c) shows the weighted ϕ distribution for events with $\cos\theta^*$ selection along with the curve corresponding to this value of μ_{Σ^+}.

VI. SYSTEMATIC ERRORS

The small-angle decay loss described in Sec. V is a possible source of systematic error in the experiment. Figure 10 shows the magnetic moments for events with $\cos\theta^*$ selection from the four field maps (open points) and for the final combined sample (full point). In Fig. 10(a) the results are plotted for method (a), with no correction for losses; Fig. 10(b) shows the results for method

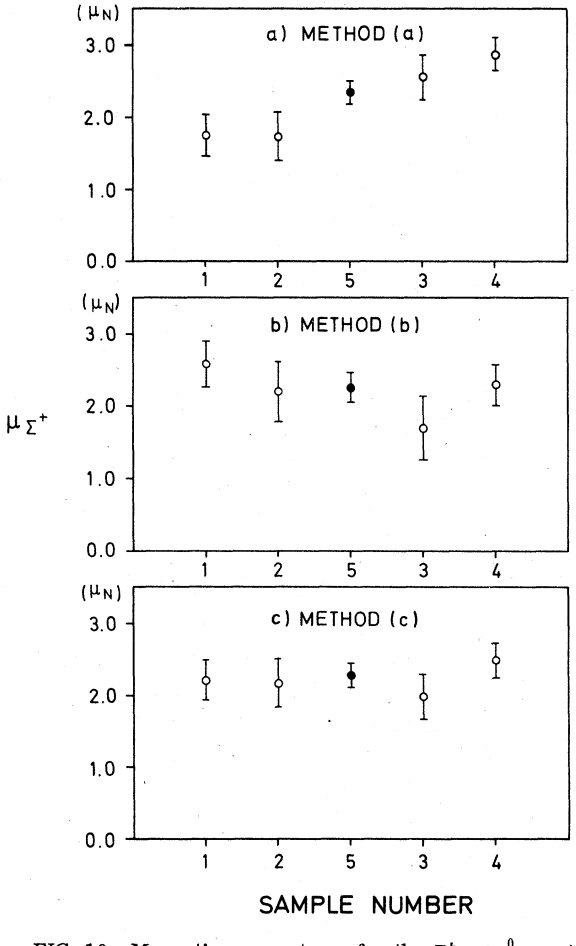

FIG. 10. Magnetic moment μ_{Σ^+} for the $\Sigma^+ \to p\pi^0$ events with $\cos\theta^*$ selection for the four field maps: 1 = positive field with opposing coil, 2 = positive field without opposing coil, 3 = negative field with opposing coil, and 4 = negative field without opposing coil. Number 5 is μ_{Σ^+} for the combined data. Values are shown for the three different methods (a), (b), and (c) for correcting for losses, as described in the text.

(b), the region of loss being cut out and the likelihood function corrected; and in Fig. 10(c) are the magnetic moments for method (c), in which the losses are corrected for by weighting the data according to a Monte Carlo calculation.

If no correction for the losses is made, method (a), then μ_{Σ^+} for a *given field direction* is biased, as can be seen in Fig. 10(a). However, the bias is in opposite directions for positive- and for negative-field samples, so that it cancels in the final sample if this sample contains equal amounts of events from the two field directions. This fact was confirmed using the aforementioned Monte Carlo calculation with a simulation of the small-angle decay losses included. Our final sample, however, has slightly different number of events with positive (6480 events) and negative (7744 events) field directions, causing the value $\mu_{\Sigma^+} = (2.35 \pm 0.14)\mu_N$ to be overestimated. To calculate this overestimate, we assigned to the negative-field events a global weight of $6480/7744 = 0.84$ in order to force the effective statistics of the two samples to be identical. That this procedure is permissible for correcting μ_{Σ^+} from method (a) was verified using the Monte Carlo calculation with simulated small-angle decay losses. It was also verified by rejecting negative-field events from the experimental data in a random fashion such that the positive- and the negative-field samples had equal statistics on the average. These procedures showed that the value is overestimated by $0.05\mu_N$. The value for method (a) then becomes $\mu_{\Sigma^+} = (2.30 \pm 0.14)\mu_N$.

The values for μ_{Σ^+} in Fig. 10(b) found by the cutting method (b) should be unbiased as long as the ϕ cuts are large enough. These cuts reduce the total number of events by 27%, so that the final error is correspondingly larger. As the cuts are varied from $\pm 0°$ [i.e., method (a)] to $\pm 40°$ about $\phi = \pm 90°$, for a *given field direction* μ_{Σ^+} changes systematically (and statistically) as the width increases up to about $\pm 20°$ beyond which the fluctuations appear to be random. The value for μ_{Σ^+} for the *final overall sample* fluctuates by $\pm 0.04\mu_N$ (rms) as a function of cut width, and these fluctuations also appear to be statistical.

The main systematic effects on the values of μ_{Σ^+} in Fig. 10(c) found by the weighting method (c) come first from the value of the magnetic moment which is used in the Monte Carlo calculation and second from the normalization of the Monte Carlo distribution to the experimental data. For the first effect we found that a $+1.0\mu_N$ change in the Monte Carlo magnetic moment produced a $+0.05\mu_N$ change in the value of μ_{Σ^+} from the maximum-likelihood fit to the weighted experimental data. The correlation is small since only a limited region of the experimental distribution is weighted. The Monte Carlo value used for μ_{Σ^+} was taken from the experimental data, for which we know μ_{Σ^+} within $\pm 0.14\mu_N$. If the Monte Carlo value for μ_{Σ^+} were off by this much, it would cause the value of μ_{Σ^+} for method (c) to be off by $0.14\mu_N \times (0.05\mu_N/1.0\mu_N) = 0.007\mu_N$. This is an estimate for the systematic error due to the first effect. For the second effect, we found that a 5% change in the normalization of the Monte Carlo distribution changed μ_{Σ^+} for a given sample (thus, for a given field direction) by $0.06\mu_N$. Unlike the first effect above, a mistake in the normalization biases μ_{Σ^+} for opposite field directions in the opposite sense, so that a systematically wrong estimation of the normalization would practically cancel when all data are collected. To check this point, the normalization was increased (then decreased) by 5% for all samples, and μ_{Σ^+} for the final combined sample changed by $\pm .01\mu_N$. This is an estimate for the systematic error due to the second effect. Confidence that the final normalization used was good is given by determining the branching ratio of the $\Sigma^+ \to p\pi^0$ decay to the $\Sigma^+ \to n\pi^+$ decay. This ratio for our weighted data is[16] $N(\Sigma^+ \to p\pi^0)/N(\Sigma^+ \to n\pi^+) = 1.05 \pm 0.01$, in good agreement with the world average[13] of 1.07 ± 0.03. For this calculation we also corrected for the small-angle decay losses in the $\Sigma^+ \to n\pi^+$ decay, but they are small, i.e., $\approx 1\%$, because this decay is practically isotropic in the bubble chamber.

Another possible source of bias is systematic errors in the measurement of the decay vertex. The production vertex is the intersection of three tracks and is therefore well measured. The decay vertex on the other hand is the intersection of only two tracks with possibly a small angle between them, and its measurement may be a problem. If, for example, the decay vertex were systematically estimated to be closer to the production vertex than it should be, the length, the $c\tau$, and hence the turning angle of the Σ^+ would all be underestimated. Since the direction of the decay proton reflects the actual polarization direction, the precession angle ϕ_0 would be overestimated. This would mean that in calculating μ_a from Eq. (5), an overestimated ϕ_0 would appear in the numerator and an underestimated $c\tau$ in the denominator, thus compounding the overestimation of μ_a. This picture is somewhat oversimplified because the HYDRA geometry uses both vertex and track measurements to estimate the vertex position and the HYDRA kinematics combines all track measurements to produce the final multivertex fit. Nevertheless the position of the decay vertex is a crucial quantity in the measurement of μ_a, and this effect is not canceled by combining positive-and

negative-field samples. It is only canceled if the numbers of underestimations and overestimations of the Σ^+ length are the same. If the lifetime measured in this experiment agrees with the world average, then we have confidence that there is no systematic error in measuring the position of the decay vertex. Using the magnetic-moment sample of 14 224 $\Sigma^+ \to p\pi^0$ events to measure the Σ^+ lifetime, we find[16] $c\tau = 2.41 \pm .02$ cm. This number was calculated making the standard[17] corrections for the Σ^+ potential path length and for the loss of short Σ^+'s. The world average[13] is 2.404 ± 0.015 cm so that on average we have correctly determined the decay vertex. Another crosscheck comes from the comparison of the lifetime calculated from our $\Sigma^+ \to p\pi^0$ and $\Sigma^+ \to n\pi^+$ sample. For the latter decay, the decay pion makes a large angle with respect to the Σ^+ on the average, so that the measurement of the decay vertex is much less problematic. Our $\Sigma^+ \to n\pi^+$ sample yields the result[16] $c\tau = 2.40 \pm 0.02$ cm, increasing our confidence in the magnetic-moment sample.

A final test on the internal consistency of our data with regard to the lifetime $c\tau$ is shown in Fig. 11. There the data have been divided up into $c\tau$ bins such that the error on μ_{Σ^+} is about the same for each bin (lower plot). The precession angle ϕ_0, Eq. (5), is plotted for each bin (upper plot), and a straight line corresponding to $\mu_{\Sigma^+} = 2.30\mu_N$ has been drawn for comparison [since method (a) was used for this plot]. The data are seen to agree well.

The systematic error due to a wrong absolute calibration of the magnetic field by 1% would be $0.02\mu_N$. The absolute field calibration was tuned to the Σ^+ mass, using the missing mass between the K^- and the π^- at the production vertex, and this mass is correct to 1 MeV/c^2 or better. This means that the actual uncertainty in the magnetic field calibration is approximately 0.1%, corresponding to a systematic error of $0.002\mu_N$.

We have also searched for possible biases as a function of the following: laboratory (MPI or VU), different partial-wave analyses[14] for computing the magnitude of the Σ^+ polarization, beam momentum, position of the event in the chamber, Σ^+ production angle, the number of degrees of freedom in the multivertex fit, and film quality. The value for μ_{Σ^+} showed only fluctuations compatible with statistical ones. Taking laboratory as an example, the film was independently scanned and measured in the two laboratories, and the results obtained are in excellent agreement: $\mu_{\Sigma^+} = (2.32 \pm 0.19)\mu_N$ and $\mu_{\Sigma^+} = (2.29 \pm 0.23)\mu_N$ after balancing the numbers of positive- and negative-field events. Taking as another example, the Σ^+ polarization, not only was μ_{Σ^+} insensitive to the partial-wave analysis used, it also did not matter whether or not the decay asymmetry parameter α was allowed to vary during the maximum-likelihood fitting (in principle the parameters μ_{Σ^+} and αP are uncorrelated).

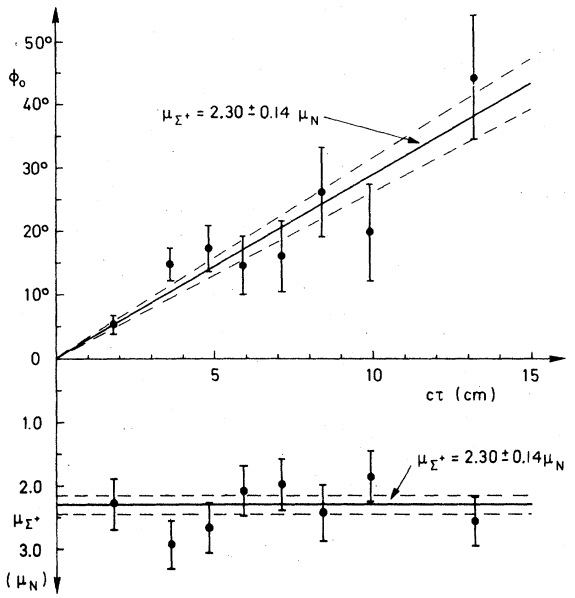

FIG. 11. Variation μ_{Σ^+}, lower plot, and of ϕ_0, upper plot, as a function of Σ^+ lifetime $c\tau$. For this plot method (a) as described in the text was used for correcting for losses. The solid straight line corresponds to the value for method (a), $\mu_{\Sigma^+} = 2.30\mu_N$, and the dotted straight lines correspond to the error on this value $\pm 0.14\mu_N$.

As mentioned previously, the measurement precision in HYBUC corresponds to a point reconstruction accuracy of 70μ in space and to a ϕ angle measuring accuracy of $\pm 1°$. The Σ^+ mass is measured to an accuracy of ± 10 MeV/c^2 for a given event. This high measurement precision was essential in reducing to a negligible level the contamination of the $\Sigma^+ \to p\pi^0$ sample with misidentified $\Sigma^+ \to n\pi^+$ decays or with proton elastic scatter events. A large error in measuring ϕ would have led to an apparent depolarization in the ϕ distribution. We calculated the apparent depolarization as a function of ϕ, including in the calculation the uncertainty in the Σ^+ turning angle (caused by the uncertainty in the Σ^+ length measurement) and the errors on measured angles and momenta as delivered by the kinematics program. We conclude that this depolarization effect is an order of magnitude too small to be detected with the present statistics.

A preliminary value[18] for μ_{Σ^+} was published using part of the data from two of the eight subsamples mentioned above. Since then, the rest

of the data has been added, additional ionization decisions have been implemented, and the optical and magnetic-field constants and the geometry-kinematics programs have been further improved. These improvements changed the value of μ_{Σ^+} for the two subsamples used for the preliminary result, which was found using method (a), to $2.76 \pm 0.28 \mu_N$, a decrease in the central value of $0.19 \mu_N$. The error attached to the preliminary value was $0.31 \mu_N$, which was purely statistical. Now we have better insight into our systematic effects, and the imbalance in numbers of positive- and of negative-field events alone leads to μ_{Σ^+} for these subsamples being overestimated by about $0.1 \mu_N$. Thus our preliminary value showed a fluctuation to the high side, this fluctuation being partly statistical and partly systematic and now understood.

Summarizing then the results after our studies on systematic effects in the data, the final value for method (a) is $\mu_{\Sigma^+} = (2.30 \pm 0.14) \mu_N$, for method (b) $\mu_{\Sigma^+} = (2.26 \pm 0.17) \mu_N$, and for method (c) $\mu_{\Sigma^+} = (2.29 \pm 0.14) \mu_N$. This bias due to the small-angle decay loss which affects only method (a) via an imbalance in the numbers of positive- and negative-field events has been calculated and the value of μ_{Σ^+} corrected for it. All other systematic effects we could find are an order of magnitude smaller than the statistical error. We therefore quote only the statistical error and avoid any of the problems associated with combining random and systematic effects.

The three methods for correcting for losses in the data yield μ_{Σ^+} values which agree well. We consider methods (b), cutting in ϕ, and (c), weighting by Monte Carlo, as giving crosschecks on the data analysis and a better understanding of systematic effects. Method (a), for which nothing is done except to balance the relative numbers of positive- and negative-field events, involves the least manipulation of the data and is therefore, after all is said and done, the one we prefer. Using the result of method (a), our final value is $\mu_{\Sigma^+} = (2.30 \pm 0.14) \mu_N$.

VII. FINAL RESULT AND DISCUSSION

As explained above, our final result is $\mu_{\Sigma^+} = (2.30 \pm 0.14) \mu_N$. The seven published measurements[7] of μ_{Σ^+} prior to the HYBUC experiment gave[19] a world average of $\mu_{\Sigma^+} = (2.62 \pm 0.41) \mu_N$. If we combine the previous results with our final value, thereby assuming that the different μ_{Σ^+} measurements fluctuate statistically, we find a new world average of $\mu_{\Sigma^+} = (2.33 \pm 0.13) \mu_N$.

A complete review of theoretical predictions for comparison with this new world average is outside the scope of this experimental paper. However, a look at how this result relates to some popular ideas as sketched in the Introduction is interesting and easy to do. Simple SU(3) and SU(6) theories,[1,2] which assume the electromagnetic interaction to transform as a U-spin scalar and the mass-splitting, symmetry-breaking interaction to be negligible, give $\mu_{\Sigma^+} = \mu_p = 2.79 \mu_N$. That the experimental value deviates by 3 standard deviations from this prediction is not surprising since the assumption about the mass-splitting interaction is manifestly wrong, as can be seen by looking at the baryon masses. Nevertheless, the present measurement of μ_{Σ^+} is firm evidence that mass splitting effects similar to those observed in the Λ^0 magnetic moment[13,20] are also present in the Σ^+ magnetic moment.

The same arguments hold for the simplest quark model,[2] in which the magnetic moment of a baryon is a simple vector sum of the quark magnetic moments over the quark wave function of the baryon, the masses of the u, d, and s quarks being the same.

A more sophisticated model[3,4] assumes that the splitting in the masses of the u, d, and s quarks is responsible for the symmetry breaking in SU(3). This gives a mechanism[4] which contributes in an important way to generating the hadron mass spectra, and it causes the baryon magnetic moments to be different from those of the simple model. For u- and s-quark masses of 333 and 510 MeV/c^2, respectively, this model finds $\mu_{\Sigma^+} = 2.67 \mu_N$. This prediction differs little from that of the simplest model because the s quark contributes with a weight of only 11% to μ_{Σ^+}. The new world average for μ_{Σ^+} still deviates by 2 standard deviations from this prediction. In fact the new world average agrees better with a "mass-corrected theory"[21] in which the simple prediction $\mu_{\Sigma^+} = \mu_p$ is to be understood in intrinsic magnetons, so that $\mu_{\Sigma^+} = 2.79$ i.m. $= 2.20 \mu_N$. The mass-corrected theory, however, is in disagreement with the Λ^0 magnetic moment.

ACKNOWLEDGMENTS

Many people have contributed to the success of this experiment. At the Max-Planck-Institut für Physik und Astrophysik, K. Gottstein deserves special recognition for his initiative in starting the HYBUC project, and we thank N. Schmitz for his continuing support. The active interest of the late W. Heisenberg was greatly appreciated. V. Scheuing made a major contribution during the construction and assisted in the testing of HYBUC in the early phases of the experiment. E. Dahl-Jensen and I. Dahl-Jensen (Niels Bohr Institute,

Copenhagen) helped to design and tune the K^- beam. At Vanderbilt University, H. Fenker has our thanks for his participation in the data analyses. D. Coffey (AMI), A. D. McInturff (BNL), and C. Whetstone were instrumental in designing and building the superconducting magnet. At CERN, the support of Ch. Peyrou and F. Schmeissner was essential for the success of the data taking phase of the HYBUC experiment. The BEBC group, the PS group, the film developing group, the cryogenics group, and the HYDRA program group (specific persons from the different groups we wish to mention are G. Linser, G. Orlic, A. Poppleton, and F. Bruyant) deserve thanks for their ready help. The experiment would not have been possible without the proficiency of the MPI technical department (here we wish to mention H. Fessler, K. Baumer, G. Bronold, O. Geist, H. Klaus, J. Osthoff, J. Ritzer J. Rodoschegg, P. Sawallisch, E. Schenk, W. Tribaneck, and E. Wolf), and we also thank the VU Science Shop (H. Carlton) for the construction of the magnet coil form. Finally, thanks go to the scanning and measuring staffs at both the Max-Planck-Institut für Physik und Astrophysik and at Vanderbilt University for their diligent work; in particular G. Waters and B. Leupold (MPI) and A. Koshakji (VU) handled the bookkeeping and processing of the exceptionally large amounts of data. This work was supported by the Bundesministerium für Forchung und Technologie of the Federal Republic of Germany and by the National Science Foundation of the U.S.A. under Grant No. 073-08392.

---

*Now at IABG, München, Germany.
†Now at III. Physikalisches Institut, Technische Hochschule, D-51 Aachen, Germany.
‡Visitor from FUCSAV, Na Slovance 2, CS-Prague 8, Czechoslovakia.
§Now at CERN, SPS Division, CH-1211 Geneva 23, Switzerland.
¶Also at CERN, EP Division, CH-1211 Geneva 23, Switzerland.

[1]Sidney Coleman and Sheldon Lee Glashow, Phys. Rev. Lett. 6, 423 (1961).
[2]M. A. B. Bêg, B. W. Lee, and A. Pais, Phys. Rev. Lett. 13, 514 (1964); W. Thirring, in *Weak Interactions and Higher Symmetries*, proceedings of the III Schladming Conference on Nuclear Physics, edited by P. Urban (Springer, Berlin, 1965),[Acta Phys. Austriaca Suppl. II, 205 (1965)].
[3]H. R. Rubinstein, F. Scheck, and R. H. Socolow, Phys. Rev. 154, 1608 (1967); J. Franklin, *ibid.* 172, 1807 (1968).
[4]A. De Rújula, H. Georgi, and S. L. Glashow, Phys. Rev. D 12, 147 (1975); H. J. Lipkin, Phys. Rev. Lett. 41, 1629 (1978).
[5]V. Bargmann, L. Michel, and V. L. Telegdi, Phys. Rev. Lett. 2, 435 (1959).
[6]Ph. Rosselet, Helv. Phys. Acta 38, 691 (1965).
[7]A. D. McInturff and C. E. Roos, Phys. Rev. Lett. 13, 246 (1964); V. Cook, T. Ewart, G. Masek, R. Orr, and E. Platner, *ibid.* 17, 223 (1966); C. R. Sullivan, A. D. McInturff, D. Kotelchuck, and C. E. Roos, *ibid.* 18, 1163 (1967); D. Kotelchuck, E. R. Goza, C. R. Sullivan and C. E. Roos, *ibid.* 18, 1166 (1967); J. Combe, E. Dahl-Jensen, N. Doble, D. Evans, L. Hoffmann, P. Rosselet, W. Toner, W. M. Gibson, K. Green, P. Tolun, N. A. Whyte, G. Charrière, M. Gailloud, B. Wanders, R. Weill, C. Carathanassis, W. Püschel, V. Scheuing, R. Settles, G. Baroni, A. Manfredini, G. Romano, and V. Rossi, Nuovo Cimento 57A, 54 (1968); T. S. Mast, L. K. Gershwin, M. Alston-Garnjost, R. O. Bangerter, A. Barbaro-Galtieri, J. J. Murray, F. T. Solmitz, and R. D. Tripp, Phys. Rev. Lett. 20, 1312 (1968); P. W. Alley, J. R. Benbrook, V. Cook, G. Glass, K. Green, J. F. Hague, and R. W. Williams, Phys. Rev. D 3, 75 (1971); M. Saha, J. G. Fetkovich, W. Heintzelmann, C. Meltzer, and C. T. Murphey, *ibid.* 7, 3295 (1973).
[8]W. H. Bergmann, J. Gruber, G. Hahn, G. Harigel, P. Meyer, K. Moustafa, and H. Röhm, Nucl. Instrum. Methods 20, 116 (1963).
[9]R. Armenteros, P. Ballion, C. Bricman, M. Fero-Luzzi, D. E. Plane, N. Schmitz, E. Burkhardt, H. Filthuth, E. Kluge, H. Oberlack, R. R. Ross, R. Barloutaud, P. Granet, J. Meyer, J. P. Porte, and J. Prevost, Nucl. Phys. B14 91 (1969).
[10]D. Coffey, A. Manz, R. Settles, S. Reucroft, and C. E. Roos, Nucl. Instrum. Methods 150, 377 (1978).
[11]Trademark, 3M company.
[12]HYDRA Application Library, CERN/EP Division, 1976 (unpublished); W. Matt, Dissertation, Technische Universität München, Max-Planck-Institut für Physik und Astrophysik Report No. MPI-PAE/Exp. El. 50, 1975 (unpublished).
[13]Particle Data Group, Phys. Lett. 75B, 1 (1978).
[14]V. Hepp, O. Braun, H. J. Grimm, H. Ströbele, C. Thöl, T. S. Thouw, F. Gandini, C. Kiesling, D. E. Plane, and W. Wittek, Phys. Lett. 65B, 487 (1976); G. P. Gopal, R. T. Ross, A. J. Van Horn, A. C. McPherson, E. F. Clayton, T. C. Bacon, and I. Butterworth, Nucl. Phys. B119, 362 (1976).
[15]S. Reucroft, C. E. Roos, J. W. Waters, M. S. Webster, T. Hansl, I. Herynek, A. Manz, J. Marraffino, W. Matt, R. Settles, and G. Wolf, Phys. Rev. D 15, 5 (1977); T. Hansl, A. Manz, W. Matt, S. Reucroft, R. Settles, J. W. Waters, G. Wolf, H. Fenker, J. M. Marraffino, C. E. Roos, and M. S. Webster, Nucl. Phys. B132, 45 (1978).
[16]Preliminary result; final result to be reported separately.
[17]R. Barloutaud, A. De Belleton, P. Granet, J. Meyer, J. P. Porte, J. Prevost, R. Armenteros, P. Baillon, C. Bricman, M. Ferro-Luzzi, J. O. Peterson, D. E. Plane, N. Schmitz, E. Burkhardt, H. Filthuth,

E. Kluge, H. Oberlack, and R. R. Ross, Nucl. Phys. B14, 153 (1969).
[18]N. Doble, K. Gottstein, T. Hansl, I. Herynek, A. Manz, J. Marraffino, W. Matt, R. Settles, G. Wolf, E. Dahl-Jensen, I. Dahl-Jensen, S. Reucroft, C. E. Roos, J. Waters, and M. S. Webster, Phys. Lett. 67B, 483 (1977).
[19]Particle Data Group, Rev. Mod. Phys. 48, S1 (1975).
[20]L. Schachinger, G. Bunce, P. T. Cox, T. Devlin, J. Dworkin, B. Edelman, R. T. Edwards, R. Handler, K. Heller, R. March, P. Martin, O. E. Overseth, L. Pondrom, M. Sheaff, and P. Skubic, Phys. Rev. Lett. 41, 1348 (1978).
[21]M. A. B. Bég and A. Pais, Phys. Rev. 137, B1514 (1965).

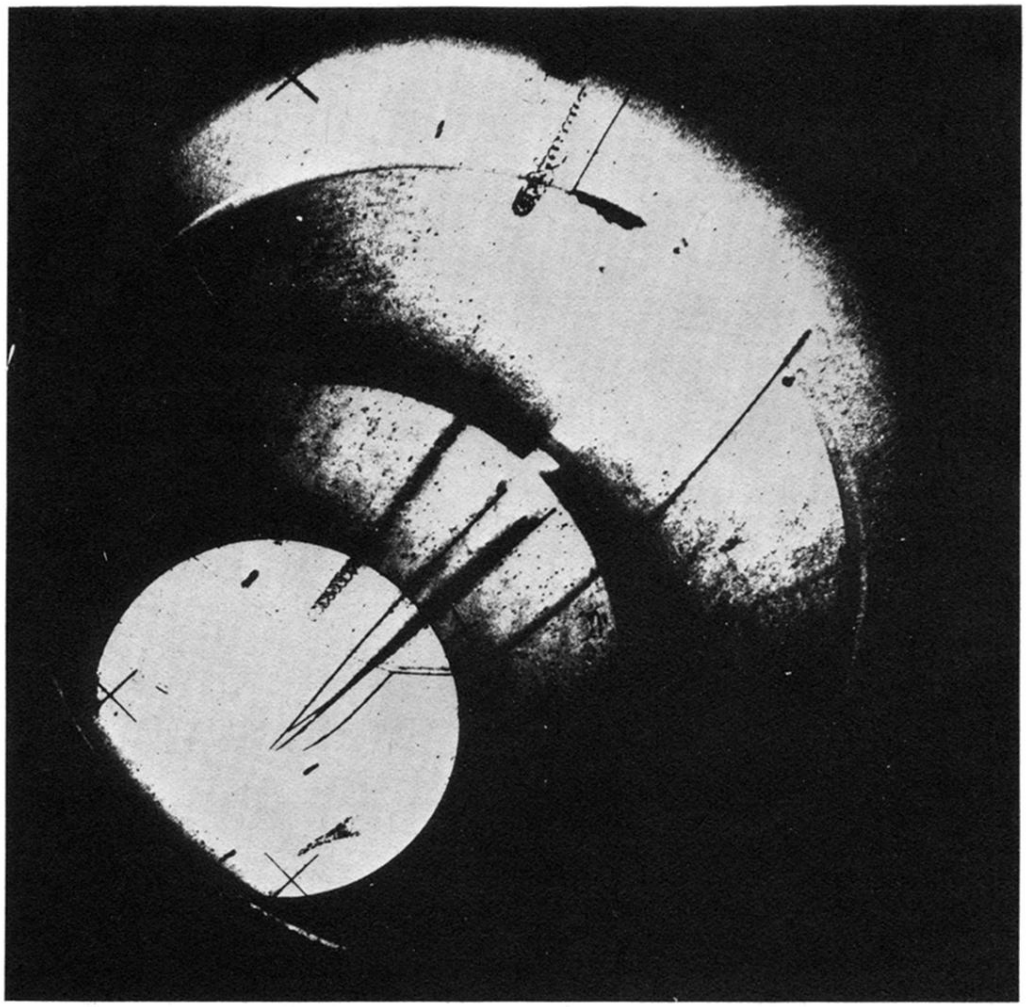

FIG. 3. A typical $K^- p \rightarrow \Sigma^+ \pi^-$, $\Sigma^+ \rightarrow p \pi^0$ event in HYBUC.